ISSN: 0067-2904

Theoretical and Experimental Study for Corrosion Inhibition of Carbon Steel in Salty and Acidic Media by A New Derivative of Imidazolidine 4-One

Nada Mohammed Al-Joborry, Rehab Majed Kubba*
Department of Chemistry, College of Science, University of Baghdad, Baghdad, Iraq

Received: 11/9/2019 Accepted: 19/11/2019

Abstract

A new imidazolidine 4-one derivative, of namly 2-[2-(4-Bromo-phenyl)-imidazo [1,2-a] pyridine-3-yl]-3-(4-nitro-phenyl)-imidazolidine-4-one (BPIPNP) was investigated as corrosion inhibitor for carbon steel in salty (3.5% NaCl) and acidic (0.5M HCl) solutions using potentiometric polarization measurements. The results revealed that the percentage inhibition efficiencies (%IE) in the salty solution (90.67%) are greater than that in the acidic solution (83.52%). Experimentally, the thermodynamic parameters obtained have supported a physical adsorption mechanism and which followed Langmuir adsorption isotherm. Density Functional Theory (DFT) of quantum mechanical method with B3LYP 6-311++G (2d, 2p) level was used to calculate geometrical structure, physical properties and inhibition efficiency parameters, in vacuum and two solvents (DMSO and H_2O), all at the equilibrium geometry. The surface changes of carbon steel were studied using Scanning Electron Microscopy SEM and Atomic Force Microscopy (AFM) techniques.

Keywords: Imidazolidine; Corrosion inhibitors; Quantum chemical calculations; Thermodynamic parameters

دراسات نظرية وتجريبية على إمكانية تثبيط مشتق جديد لإيميدازولدين 4-أون لتآكل حديد الصلب الكربوني في الوسطين الملحي والحامضي

ندي محمد الجبوري، رحاب ماجد كبة *
قسم الكيمياء كليةالعلوم، جامعة بغداد، بغداد، العراق

الخلاصه

تم فحص المشتق (limidazolidine 4-one) ، الذي يحمل الاسم:
2-[2-(4-Bromo-phenyl)-imidazo [1,2-a] pyridine-3-yl]-3-(4-nitro-phenyl)-imidazolidine-4-one (BPIPNP) كمثبط لتآكل لحديد الصلب الكربوني في المحلول الملحي (3.5٪ كلوريد الصوديوم) والحامضي (0.5 M حمض الهيدروكلوريك) باستخدام قياسات الاستقطاب المجهادي. أظهرت النتائج أن النسبة المؤية لكفاءة التثبيط (%IE) في المحلول الملحي (90.67%) أكبر منها في المحلول الحامضي (83.52%). ومن الناحية التجريبية، تدعم المعلمات الديناميكية الحرارية التي تم الحصول عليها آلية الامتزاز الفيزيائي وأن امتزازه على سطح حديد الصلب الكربوني يطيع ايزوثيرم امتزاز لنكماير

*Email: Rehab_mmr_kb@yahoo.com

Langmuir. وقد تم استخدام طريقة حسابات ميكانيك الكم وفق نظرية دوال الكثافة (DFT) عند المستوى (2d,2p) 6−311++G (B3LYP) لحساب البنية الهندسية والخصائص الفيزيائية ومعاملات كفاءة التثبيط في الفراغ و في المذيبين (DMSO) و (H_2O)، وكل ذلك تم عند الشكل الهندسي التوازني. وتمت دراسة التغيرات السطحية للفولاذ الكربوني باستخدام تقنيتي (SEM) الفحص المجهري للإلكترون و (AFM) الفحص المجهري للقوة الذرية.

1. Introduction

Corrosion is an undesirable phenomena occur because chemical or electrochemical reactions between a metal and its environment. It is a spontaneous process including decrease in Gibb's free energy [1]. In spite of that corrosion process is not completely avoid but there are many methods to inhibit it. One of these methods are using inhibitors, inhibitor is a substance added in a small concentration to corrosive media causes decrease in corrosion rate of the area that exposed to that environment [2]. Many of inhibitors that used in industry are organic heterocyclic compounds [3]. Organic heterocyclic inhibitors usually have hetero atoms. The type of mechanism that inhibitors applied was adsorption mechanism, these inhibitors forming a preventative film on the metal surface.
Quantum chemical calculations were used to study the reaction mechanism and to solve chemical ambiguities. The structural and electronic parameters of the inhibitors molecules can be obtained by theoretical calculations using computational methodologies of quantum chemistry [4].
In this research we focused on the Imidazo[1,2-a]pyridine derivative (BPIPNP), a heterocyclic entities and pharmacologically important molecule, Figure-1. Several procedures for their synthesis have been studied [5].

The aim of this work is to study the inhibition efficiency of the organic inhibitor (BPIPNP) which was prepared by Naeemah Al-Lami et. al [6]; experimentally, in salty (3.5% NaCl) and acidic (0.5M HCl) solutions using potentiostatic method, and theoretically, the calculations were done in three media (vacuum, DMSO, and water) depending on quantum mechanical parameters using DFT method with [6-311/ B3LYP++G (2d, 2p)] level using Gaussian 09 program.

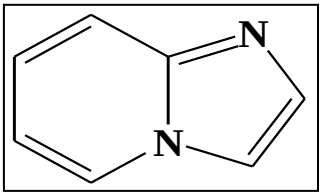

Figure 1-Structure of imidazo [1,2-a] pyridine.

2. Experimental details

2.1. Preparation of carbon steel samples

Carbon steel's rod is symbolized as (C45) with the following percentage of metallic materials in composition (wt %): (0.122% C, 0.206% Si, 0.641% Mn, 0.016% P, 0.031% S, 0.118% Cr, 0.02% Mo, 0.105% Ni, and 0.451% Cu) [7]. The rod mechanically cutting in to pieces forming a disk specimen of carbon steel a with 1.6 cm diameter and 3 mm thickness, each of these specimen was refined with emery paper (silicon carbide SiC) in different grades (80, 150, 220, 320, 400, 1000, 1200 and 2000), then washed with tap water, distilled water and degreased with acetone, washed again with deionizer water, and finally held in a desiccators after it is dried at room temperature.

2.2. Preparation of solutions

2.2.1. Blank of the salt solution

35 gm of (NaCl salt) was dissolved in (100 ml) distal water; transferred the formative solution in to (1000ml) volumetric flask, which contained (6ml) of dimethyl sulfoxide (DMSO) solvent. The volume of the solution was completed to (1L) by adding distal water.

2.2.2. Acid blank solution

40 ml (~0.5M) of HCl was diluted by distilled water to (1liter) in a volumetric flask, after adding (6ml) of the solvent of dimethyl sulfoxide (DMSO).

2.2.3. Preparation the salty solutions of 2-[2-(4-Bromo-phenyl)-imidazo [1,2-a] pyridine-3-yl]-3-(4-nitro-phenyl)-imidazolidine-4-one (BPIPNP)

Three concentrations of the (BPIPNP) inhibitor (5, 10 and 20) ppm were prepared by dissolving (0.005, 0.01 and 0.02) gm, respectively in 6ml (DMSO), then each one transferred to (1L) volumetric flask containing 35g (3.5% NaCl) dissolved in distal water. The volume of each solution was completed to (1L) with the distilled water.

2.2.4. Preparation the acidic solutions of 2-[2-(Bromo-phenyl)-imidazo [1,2-a] pyridine-3-yl]-3-(4-nitro-phenyl)-imidazolidine-4-one (BPIPNP)

Three concentrations of (BPIPNP) inhibitor (5, 10 and 20) ppm were prepared, by dissolving (0.005, 0.01 and 0.02) gm, respectively in (6ml) DMSO, then transferred each one to (1L) volumetric flask containing (40ml) HCl. The volume for each solution was completed to (1L) with the distilled water.

2.3. Electrochemical measurements

Potentiostatic polarization study

The potentiostat set up has included the following: a host computer with Mat lab software (Germany, 2000) magnetic stirrer, thermostat. The main part of the apparatus is the corrosion cell; which was made out of Pyrex with 1L capacity. This cell consisted of two bowls external and internal. Three electrodes are mainly present in the electrochemical corrosion cell. Carbon steel specimen with ($1cm^2$) surface area represented the working electrode. This is used to determine the working electrode potential due to another electrode namely as reference electrode, located closed to working electrode. A reference electrode was silver-silver chloride (Ag/AgCl, 3.0M KCl). The auxiliary electrode is a platinum rode electrode with (10cm) length. The starting step was represented in immersing the working electrode in the test solution for fifteen minutes (15min), to establish a steady state open circuit potential (E_{ocp}). This potential was noted for starting the electrochemical measurements in the range of (±200 mV). All tests solutions were conducted at temperatures of (293, 303, 313 and 323) K.

2.4. Results and discussion

Quantum chemical calculations

Quantum chemical methods are an important ways in electrochemistry studies, it's represented as the fastest ways for studying the structural nature of organic compounds specially those used as inhibitors and described how these inhibitors inhibited corrosion. The efficiencies of corrosion inhibitors are investigated by theoretically parameters of corrosion inhibition such as the energy of the Highest Occupied Molecular Orbital (E_{HOMO}), the energy of the Lowest Unoccupied Molecular Orbital (E_{LUMO}), the energy gap ($\Delta E_{HOMO-LUMO}$) between E_{HOMO} and E_{LUMO}, electro negativity (χ), dipole moment (μ) electron affinity (A), ionization energy (IP), softness (s), global hardness (η), global electrophilicity (ω), and the fraction of transferred electrons (ΔN) [8].

Molecular geometry

The organic inhibitor compound was built using Chem. Draw of MOPAC program, see Figure-(2a). Gaussian 09 packages were used for calculating the fully optimize structure [9], see Figure- (2b), using DFT (Density Functional Theory) method of Becke's three-parameter of Lee, Yang and Parr (B3LYP) with a 6-311++G (2d, 2p) level of theory [10]. In addition to vacuum, the equilibrium geometry was calculated in two solvents of (DMSO and H_2O).

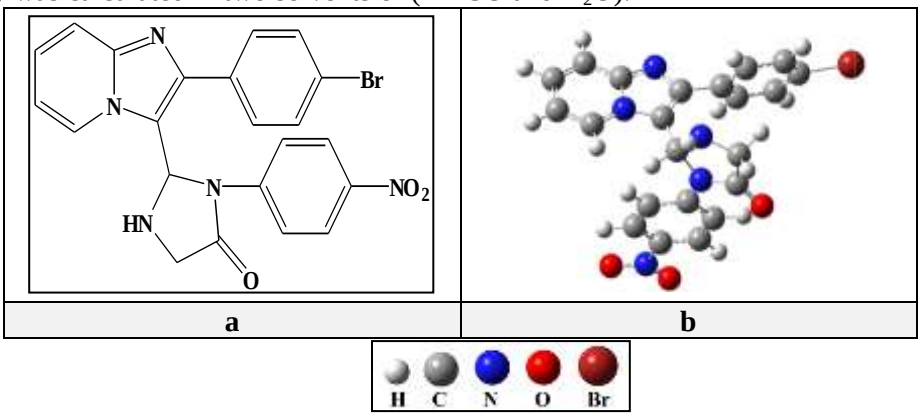

Figure 2- a. The two dimension **s**tructure of (BPIPNP) and **b.** The three dimension optimize structure of the imidazolidine 4-one derivative (BPIPNP).

Table-1 displays the geometrical structure of compound BPIPNP**,** such as bond lengths, bond angels and dihedral angles, in vacuum and two solvents (DMSO and H_2O) which calculated using DFT method. According to this table, the C13-Br (1.91625Å) is the longest bond length and N20-H (1.00617Å) is the shortest bond length for BPIPNP compound. The bond angles are in the range of (104.9640A°) for N4C7C8 to (133.43473A°) for C8C7C16. The values of the dihedral angles (trans & cis) proven that the compound is not planar with point group of C_1 [the cis dihedral angles aren't 0.0 degree and all of the trans dihedral angles are more or less than 180.0 degree]. Figure-3 shows the numbering of atoms of compound (BPIPNP).

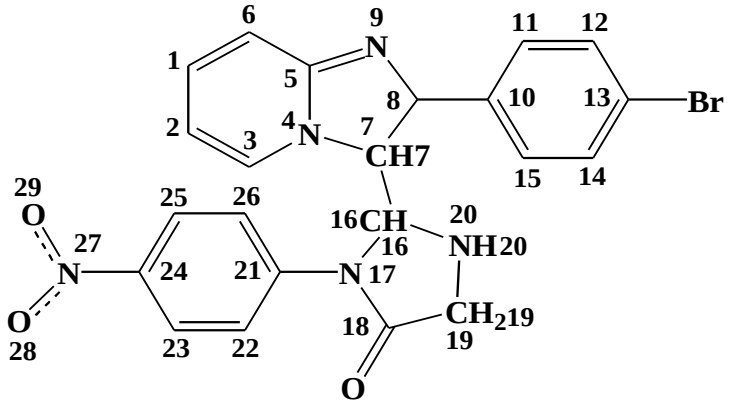

Figure 3-The numbering of atoms of compound BPIPNP.

Table 1- The geometrical structure of compound BPIPNP in vacuum and (DMSO, H_2O) solvents as calculated by DFT method.

Description bond length	Bond length (Å)	Description angle	Angle (^{0})	Description dihedral angle	Dihedral angle (^{0})
C1-C2	1.41816	**C2C1C6**	120.05330	**HC1C2H**	-0.47272
C1-C6	1.36782	**C1C2C3**	120.61559	**HC1C2C3**	179.90852
C1-H	1.07980	**C2C1H**	119.54669	**HC3N4C7**	1.21442
C2-C3	1.36057	**N4C3C2**	119.61941	**HC3N4C5**	-178.11901
C3-N4	1.37373	**C5N4C3**	121.19868	**C3N4C5C6**	-1.08226
N4-C5	1.40480	**C5N4C7**	106.45645	**C3N4C5N9**	178.99516
N4-C7	1.38835	**N4C5N9**	111.08837	**N9C5C6H**	0.30675
C5-C6	1.40697	**N9C5C6**	130.05508	**N9C5C6C1**	-179.71339
C5-N9	1.32638	**C5C6C1**	119.64710	**N4C7C8N9**	-1.39675
C7-C8	1.38789	**N4C7C8**	104.96430	**N4C7C8C10**	179.14305
C7-C16	1.50123	**C8C7C16**	133.43473	**C7C8N9C5**	1.10526
C8-C10	1.47895	**C7C8N9**	111.72101	**C10C8N9C5**	-179.37517
C8-N9	1.36351	**C7C8C10**	129.04363	**C8C10C11H**	-2.39095
C10-C15	1.39621	**C8N9C5**	105.75216	**C8C10C11C12**	177.03983
C11-C12	1.38964	**C11C10C8**	120.22762	**HC12C13Br**	-0.04457
C13-Br	1.91625	**C11C10C15**	118.84712	**BrC13C14H**	0.58546
C14-C15	1.39069	**C10C11H**	119.60934	**BrC13C14C15**	-179.89461
C15-H	1.08064	**C12C13Br**	119.25321	**HC14C15C10**	179.33935
C16-N17	1.48865	**C14C15C10**	120.83553	**HC16N17C21**	62.76226
C16-N20	1.47233	**C7C16N20**	115.41856	**HC16N17C18**	-117.46091
N17-C18	1.38380	**C7C16H**	107.70962	**C21N17C18O**	-1.68290
N17-C21	1.40840	**C16N17C18**	111.94958	**C21N17C18C19**	178.96255
C18-C19	1.50883	**C16N17C21**	122.40330	**OC18C19H**	-53.68784
C18-O	1.21524	**C17C18O**	126.67677	**OC18C19N20**	-175.32958
C19-N20	1.46164	**C18C19H**	108.30103	**C18C19N20C16**	-5.80913

C19-H	1.09044	**C19N20H**	111.88765	**C18C19N20H**	117.37171
N20-H	1.00617	**C19N20C16**	109.79813	**N17C21C22H**	-0.96437
C21-C22	1.40233	**N17C21C26**	121.29083	**N17C21C22C23**	179.45793
C22-C23	1.38256	**N17C21C22**	119.57029	**HC22C23H**	0.35778
C22-H	1.07776	**C21C22C23**	120.81062	**HC22C23C24**	-179.47865
C23-C24	1.38820	**C23C24C25**	121.22076	**HC23C24N27**	0.20348
C24-C25	1.38994	**C23C24N27**	119.20980	**HC23C24C25**	-179.86564
C24-N27	1.45164	**C25C26C21**	120.09463	**N27C24C25H**	0.12946
C25-C26	1.38317	**O28N27O29**	123.70520	**N27C24C25C26**	179.78793
N27-O29	1.23669	**O29N27C24**	118.11454	**HC25C26C21**	179.88198

Figure-4 shows the geometrical optimization of the studied inhibitor in vacuum including HOMO and LUMO distributions. The HOMO is mainly located on the (2-(2-Biphenyl-4-yl-imidazo [1,2-a] pyridine-3-yl)) moiety. This indicates that the preferred actives sites for an electrophilic attack are located within the region around the nitrogen atoms. Moreover, the electronic density of LUMO was distributed at the aromatic ring and around the ring of (4-nitro-phenyl) moiety (the most planar region in the molecule).

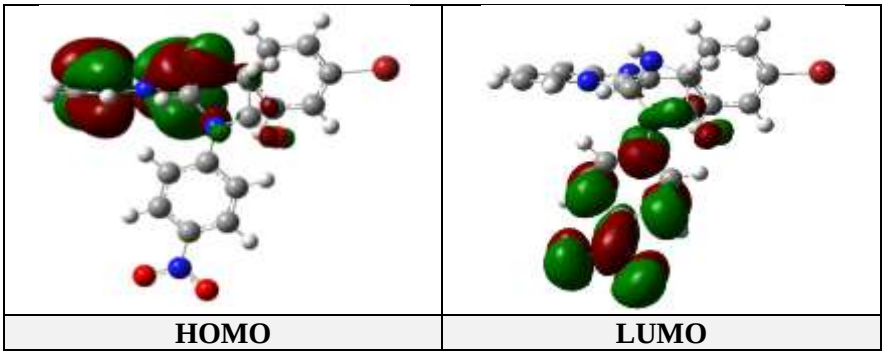

HOMO	**LUMO**

Figure 4-The Frontier molecular orbital distributions of BPIPNP compound using DFT method. [Red color: negatively charged lobe; blue color: positive charge lobe].

Global molecular reactivity

To study the influence of molecular geometry on the mechanism and efficiency of inhibition, some of the chemical quantum calculations were performed such as, the energy of highest occupied molecular orbital (E_{HOMO}), the energy of the lowest unoccupied molecular orbital (E_{LUMO}), the energy gap ($\Delta E_{HOMO-LUMO}$) and the dipole moment (μ). The other quantum chemical parameters are all shown in Tables-(2a, 2b).

The Frontier orbital theory was used in predicting the adsorption centers of the inhibitor responsible of the reaction metal surface/ molecule [11]. According to this theory, the formation of a transition state is due to an interaction between the Frontier orbital's (HOMO and LUMO) of reactants with the metal surface. The HOMO energy (E_{HOMO}) is often associated with the electron donating ability of the molecule, thus, inhibitors with high values of (E_{HOMO}) have a tendency to donate electrons to appropriate acceptor with low empty molecular orbital energy. Contrariwise, LUMO energy (E_{LUMO}) indicates the ability of molecule for electron-accepting, the lowest value of E_{LUMO}, the higher the capability of accepting electrons. The energy gap between the Frontier orbital's ($\Delta E_{HOMO-LUMO}$) is also an important factor in describing the molecular activity, so when the energy gap is decreased, the inhibitor efficiency increased [12]. Activation hardness has been also defined on the basis of the $\Delta E_{HOMO-LUMO}$ energy gap. The qualitative definition of hardness is closely related to the polarizability, since any decrease in the energy gap usually leads to easier polarization of the molecule. All these parameters which are related to the efficiency of the inhibition of a molecule, values of E_{HOMO}, E_{LUMO}, $\Delta E_{HOMO-LUMO}$, electronegativity (χ), molecular dipole moment, softness (S), global hardness (η), the fraction of electron transferred (ΔN), were calculated using the density functional theory (DFT) and have been used to understand the properties and activity of the newly prepared organic compounds and to help in the explanation of the experimental data obtained for the

corrosion process. The ionization potential (IP) and electron affinity (EA) of the inhibitors are calculated according to Koopman's theorem [13], using the following Equations [14]:

$$IP = -E_{HOMO} \quad (1)$$

$$EA = -E_{LUMO} \quad (2)$$

The electronegativity (χ) and the chemical hardness (η) according to Pearson, operational and approximate definitions can be evaluated using the following relations [14]:

$$\chi = (IP + EA)/2 \quad (3)$$

$$\eta = (IP - EA)/2 \quad (4)$$

Global chemical softness (S), which describes the capacity of an atom or group of atoms to receive electrons [9], was estimated by using Equation 5:

$$S = 1/\eta \quad (5)$$

The Global electrophilicity index (**ω**) introduced by Parr [15]. It was used for calculating the electronegativity and chemical hardness parameters, Equation 6:

$$(\boldsymbol{\omega}) = (-\chi)^2 / 2\eta = \mu^2/2\eta \quad (6)$$

The fraction of electrons transferred (ΔN) from an inhibitor molecule to the carbon steel surface was also calculated using theoretical (χ_{Fe}) and (η_{Fe}) values for mild steel of 7.0 eV mol^{-1} and 0.0 eV mol^{-1}, respectively. The number of transferred electrons (ΔN) was calculated using Equation (7) [15]:

$$\Delta N = (\chi_{Fe} - \chi_{inhib.})/[2(\eta_{Fe} + \eta_{inhib.})] \quad (7)$$

Tables-(2a, 2b) show that BPIPNP compound was a good inhibitor depending on the values of quantum chemical parameters in media (vacuum, DMSO and H_2O). E_{HOMO} in vacuum was (-6.480 eV), decreased in DMSO and H_2O solvents, the (E_{LUMO}) in the vacuum (-2.909 eV), decreased in DMSO and H_2O solvents and the value of $\Delta E_{HOMO-LUMO}$ is (3.571 eV) in vacuum, be lower in DMSO (3.118 eV) and H_2O (3.113 eV), indicating that the stability of the inhibitor in the solvents is lower than that in the vacuum.

The dipole moment (μ in Debye) is an important electronic parameter that results from the non-uniform distribution of charges on the different atoms in the molecule. The increasing in the value of dipole moment increases the adsorption between a chemical compound and metal surface [16]. Dipole moment for BPIPNP inhibitor in vacuum is (8.8305 Debye), increased in DMSO and H_2O as a result of increasing polarity of the solvent.

The ionization potential, IP can be approximated as the negative of the E_{HOMO} [17]. Low values of IE increase the effectiveness of the inhibitor. The IP of BPIPNP inhibitor in the vacuum is (6.480eV), decrease in DMSO and H_2O solvents.

EA is the amount of energy released when adding an electron to an atom or molecule [18]. A high value of EA indicates a less stable inhibitor (good corrosion inhibitor). The electron affinity of BPIPNP in the vacuum is (2.909eV), be a higher on using DMSO and H_2O solvents.

Chemical Hardness (η) is a measure of the ability of atom or molecule to transfer the charge. Increasing (η) decreases the stability of molecule, so the inhibitor possessed a high value of (η) is considered to be a good inhibitor. (η) value for BPIPNP in the vacuum is (1.785eV), be a lower in DMSO and H_2O solvents.

Chemical Softness (S) is a measure of the flexibility of an atom to receive electrons (S), Molecules having a high value of S are considered to be a good inhibitor. The values of (S) in the vacuum is (0.560 eV), increase in DMSO and H_2O.

The electronegativity (**χ**) is the ability of an atom or a group to pull electrons, High electronegativity indicates a good inhibitor [19]. The calculated (**χ**) for BPIPNP in the vacuum was found to be (4.694eV), decreased in DMSO and H_2O solvents.

Global electrophilicity index (**ω**) is the measure of the stability of an atom after gaining an electron [20], Low value of (ω) meaning the molecule has a good inhibition. In the vacuum is (6.171eV), increased in DMSO and H_2O.

ΔN (Difference in number of electrons transferred) is the fraction of electrons transferred from an inhibitor to carbon steel surface. BPIPNP has ΔN value up to (0.645) in the vacuum and increased in solvents leading to increase the ability of inhibition efficiency, when the two systems, Fe, and inhibitor, are brought together.

Table 2a- DFT calculations of some physical properties for imidazolidin-4-one derivative (BPIPNP**)** at equilibrium geometry.

Inhib. Medium	Point group	Molecular formula	E_{HOMO} (eV)	E_{LUMO} (eV)	$\Delta E_{HOMO-LUMO}$ (eV)	μ (Debye)	E_{total} (eV)
Vacuum	C_1	$C_{22}H_{18}N_5O_3Br$	-6.480	-2.909	3.571	08.8305	-106721.330
DMSO	C_1		-6.220	-3.102	3.118	12.1458	-106722.027
Water	C_1		-6.217	-3.104	3.113	12.2054	-106722.038

Table 2b- DFT quantum chemical parameters for imidazolidin-4-one derivative (BPIPNP**)** at equilibrium geometry

Inhib. Medium	IP (eV)	EA (eV)	η (eV)	χ (eV)	S (eV)	ω (eV)	ΔN
Vacuum	6.480	2.909	1.785	4.694	0.560	6.171	0.645
DMSO	6.220	3.102	1.559	4.661	0.641	6.967	0.750
Water	6.217	3.104	1.556	4.660	0.642	6.977	0.751

Active sites of the (BPIPNP) inhibitor

The inhibition of the studied inhibitors was determined using DFT Mulliken charges population analysis; which gave an indication of the reactive centers of the compounds (electrophilic centers and nucleophilic centers). For that, region that have a large electronic charge are chemically softer than the region that have a small electronic charge. Thus, the density of electron may play an important role in the chemical reactivity calculating. The chemical adsorption interactions are either by orbital interactions or electrostatic. The nucleophilic attack sites will be the place where the positive charge value is a maximum, and hence only the charges on the oxygen (O), nitrogen (N), and some carbon atoms would be presented. The electrophilic attack site was controlled by the negative charge value.

The nucleophilic and electrophilic electronic charge values of compounds are stronger in DMSO and H_2O solutions than in vacuum. Table-3 shows Mulliken charges population (ecu) analysis for the (BPIPNP**)** compound in media (vacuum, DMSO, and H_2O). According to this table, the order of the nucleophihic reactive sites of (BPIPNP**)** inhibitor is: O30> C14> C12> N9> C2> C1> C23> N20> C8> C15> C26, and the order of the electrophihic reactive sites order is: C5> C21> C10> C18.

Table 3- DFT calculations of Mulliken charges population (**ecu**) for (BPIPNP**)** molecule in media (vacuum, DMSO, and H_2O).

Atom No.	Electronic charge	Atom No.	Electronic charge	Atom No.	Electronic charge	Atom No.	Electronic charge
C_1	-0.312V -0.336D -0.337H	C_8	-0.395V -0.239D -0.236H	N_{17}	-0.103V -0.078D -0.077H	C_{25}	-0.162V -0.190D -0.190H
C_2	-0.282V -0.348D -0.349H	N_9	-0.227V -0.356D -0.354H	C_{18}	0.208V 0.257D 0.258H	C_{26}	-0.214V -0.221D -0.221H
C_3	-0.082V -0.039D -0.038H	C_{10}	0.402V 0.398D 0.398H	C_{19}	0.072V -0.074D -0.074H	N_{27}	-0.023V 0.030D 0.031H
N_4	0.155V 0.155D 0.155H	C_{11}	-0.037V -0.070D -0.070H	N_{20}	-0.257V -0.309D -0.310H	O_{28}	-0.132V -0.190D -0.191H
C_5	0.607V 0.612D 0.612H	C_{12}	-0.322V -0.361D -0.362H	C_{21}	0.465V 0.460D 0.460H	O_{29}	-0.140V -0.194D -0.195H

C_6	-0.163V -0.163D -0.163H	C_{13}	0.134V 0.098D 0.097H	C_{22}	-0111V -0.089D -0.088H	O_{30}	-0.397V -0.479D -0.480H
C_7	-0.138V -0.135D -0.135H	C_{16}	-0.060V -0.066D -0.066H	C_{23}	-0.302V -0.303D -0.303H	Br	-0.049V -0.060D -0.060H

V: vacuum, D: dimethyl sulfoxide (DMSO), W: water, ecu: electron controstatic unit.

Corrosion inhibition measurement

Potentiodynamic Polarization Measurements

The electrochemical kinetics of metallic corrosion process can be characterized by determining at least three polarization parameters, such as corrosion current density ($I_{corr.}$), corrosion potential ($E_{corr.}$) and Tafel slopes (ba and/or bc). The corrosion behaviour can be determined by a polarization curve (E versus log I). The evaluation of the polarization parameters leads to the determination of the corrosion rate (C.R). Using Tafel extrapolation method, it is possible to obtain the I_{corr} at the E_{corr} by the extrapolation of anodic and/or cathodic Tafel lines [21].

Measurements were performed in 3.5% NaCl solution and acidic solution containing different concentrations of the tested inhibitor (BPIPNP**)**. The linear Tafel segments of anodic and cathodic curves were extrapolated to corrosion potential to obtain the corrosion current densities I_{corr} and inhibition efficiency percentage IE%, Equation 8:

$$\%\mathbf{IE} = \frac{\mathrm{I_{corr(un)} - I_{corr(in)}}}{\mathrm{I_{corr(un)}}} \times 100 \quad \ldots . (\mathbf{8})$$

Where $I_{corr\ (in)}$ is the inhibited corrosion current densities, $I_{corr\ (un)}$ is the uninhibited current densities. The values of polarization resistance Rp was calculated using Equation 9 [22]:

$$\mathrm{Rp} = \frac{b_a \times b_c}{2.303(b_a + b_c) \times I_{\mathrm{corr}}} \quad (\mathbf{9})$$

The surface coverage (**Θ**) of the carbon steel corrosion immersed in 3.5% NaCl solution and acidic solution containing different (BPIPNP**)** concentration (C) could be estimated, using Equation 10:

$$\mathbf{\Theta} = \frac{\%\mathbf{IE}}{100} \quad (\mathbf{10})$$

While the corrosion rate (CR) was calculated by Equation 11:

$$\mathbf{CR} = I_{\mathrm{corr}} \times 0.249 \ldots \quad (\mathbf{11})$$

The addition of the imidazolidine 4-one derivative causing decrease in the corrosion rate, i.e. shifts of the catholic and anodic curves to lower values of current densities, and both cathodes and anodic reactions of carbon steel electrode corrosion are inhibited by the inhibitor in both 3.5% NaCl solution and acidic solution. Figure-5 shows potentiodynamic polarization curves for C.S (C45) in the salt solution, with and without the addition of (BPIPNP**)** inhibitor at various concentrations, and at the optimum conditions of (20ppm) with temperature of (293K), on the other hand, Figure-6 shows potentiodynamic polarization curves for C.S (C45) in the acidic solution with and without the addition of (BPIPNP**)** at various concentrations, and at the optimum conditions of (20ppm) with temperature of (293K).

Table-4, collects the values of corrosion rates of C.S and inhibition efficiency of inhibitor studied at various concentrations and different temperature in salt solution, while, Table-5, the values of corrosion rates of C.S and inhibition efficiency of inhibitor studied at various concentrations and different temperature in acidic solution. These tables showing that increasing temperature lead to increase the corrosion current densities $I_{corr.}$, while the efficiencies IE% enhances with the increasing the inhibitor concentration. The optimum conditions for BPIPNP in the salt solution were observed at 293K and 20ppm corresponded to lowest $I_{corr.}$ (12.41 μA.cm^{-2}) and maximum IE% (90.67%) and The optimum conditions for BPIPNP in the acidic solution were observed at 293K and 20ppm too, corresponded to lowest $I_{corr.}$(32.38 μA. cm^{-2}) and maximum IE% (83.52%). The values of iron corrosion rate CR were decreased with increasing the concentration of (BPIPNP**)** inhibitor and the addition of inhibitor to the blank solutions increased the cathodic and anodic current densities without shifting the corrosion potential, so (BPIPNP**)** inhibitor can be described as a mixed-type inhibitor. Its inhibition caused by adsorption and the inhibition effect results from the reduction of the reaction area on the surface of the carbon steel [23].

Table 4- Electrochemical data of C.S corrosion in 3.5% NaCl solution and at different concentrations of (BPIPNP**)** compound

Solu.	T (K)	E_{corr} (mV)	I_{corr} ($\mu A.cm^{-2}$)	bc ($mV.dec^{-1}$)	Ba ($mV.dec^{-1}$)	IE%	Ɵ	CR
Blank 3.5% NaCl	293	-408.0	133.13	-230.4	138.5	------	------	33.15
	303	-446.7	172.04	-279.6	110.2	------	------	42.84
	313	-491.2	189.34	-269.0	96.5	------	------	47.15
	323	-547.7	192.99	-252.9	84.4	------	------	48.05
5ppm	293	-471.6	17.07	-113.4	54.8	87.17	0.8717	4.25
	303	-509.6	22.92	-188.3	61.5	86.67	0.8667	5.71
	313	-508.9	31.76	-78.9	44.0	83.22	0.8322	7.91
	323	-558.0	34.51	-157.7	70.1	82.11	0.8211	8.59
10ppm	293	-300.3	16.09	-51.1	40.6	87.91	0.8791	4.01
	303	-472.5	34.0	-58.3	44.6	80.23	0.8023	8.47
	313	-507.9	51.78	-62.2	40.8	72.65	0.7265	12.89
	323	-520.2	69.18	-63.2	43.3	64.15	0.6415	17.23
20ppm	293	-538.6	12.41	-94.0	72.3	90.67	0.9067	3.09
	303	-486.5	25.05	-73.3	44.0	85.43	0.8543	6.24
	313	-505.7	37.58	-94.1	49.4	80.15	0.8015	9.36
	323	-523.9	42.37	-130.9	62.1	78.04	0.7804	10.55

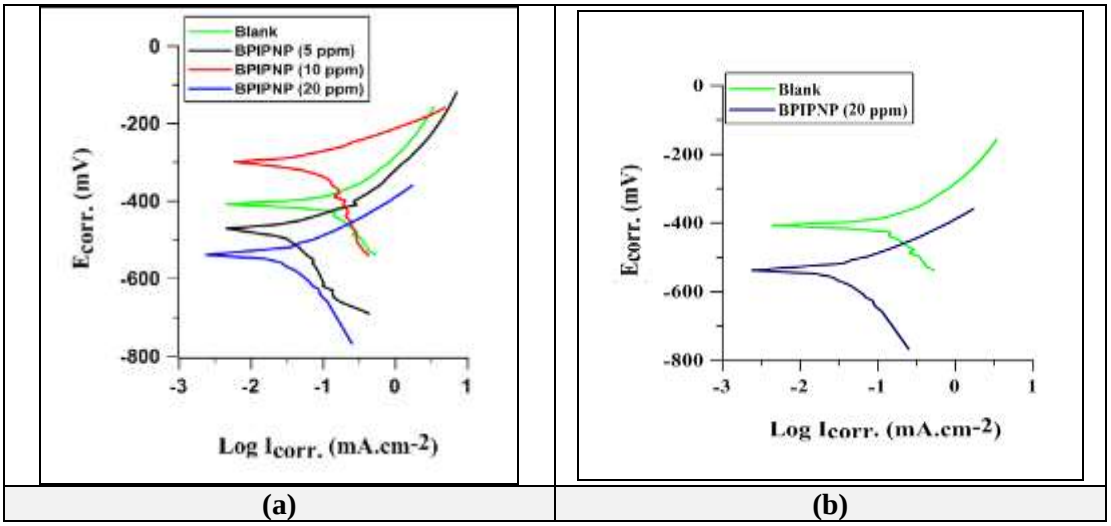

Figure 5-Polarisation curve of C.S in sea water for (BPIPNP**)** compound (a) at different concentrations at T(293K), (b) at the optimum concentration of (BPIPNP) compound at T(293K).

Table 5- Electrochemical data of carbon steel corrosion in 0.5M HCl at different concentrations of (BPIPNP**)** compound.

Solu.	T (K)	E_{corr} (mV)	I_{corr} ($\mu A.cm^{-2}$)	bc ($mV.dec^{-1}$)	Ba ($mV.dec^{-1}$)	IE%	Ɵ	CR
Blank 0.5M HCl	293	-340.2	196.59	-132.9	76.1	------	------	48.95
	303	-349.9	285.76	-129.4	87.4	------	------	71.15
	313	-336.8	383.29	-123.8	77.4	------	------	95.44
	323	-326.9	495.50	-107.5	58.6	------	------	123.38
5ppm	293	-332.6	40.67	-52.3	38.8	79.31	0.793	10.13
	303	-322.5	64.44	-42.5	46.3	77.44	0.774	16.05
	313	-328.8	118.87	-49.4	47.2	68.99	0.690	29.60
	323	-327.6	174.75	-49.2	47.6	64.73	0.647	43.51
10ppm	293	346.5-	39.48	-53.4	45.0	79.91	0.799	09.83
	303	-342.2	79.81	-44.5	51.5	72.07	0.720	19.87
	313	-335.4	119.73	53.8	44.2	68.76	0.689	29.81
	323	334.5-	177.24	-49.4	43.0	64.23	0.642	44.13
20ppm	293	-345.1	32.38	-41.9	40.8	83.53	0.835	08.06
	303	-328.0	61.94	-45.0	49.6	78.32	0.783	15.42
	313	-323.2	108.51	-53.0	48.7	71.69	0.717	27.02
	323	-324.4	141.91	-48.8	43.3	71.36	0.713	35.34

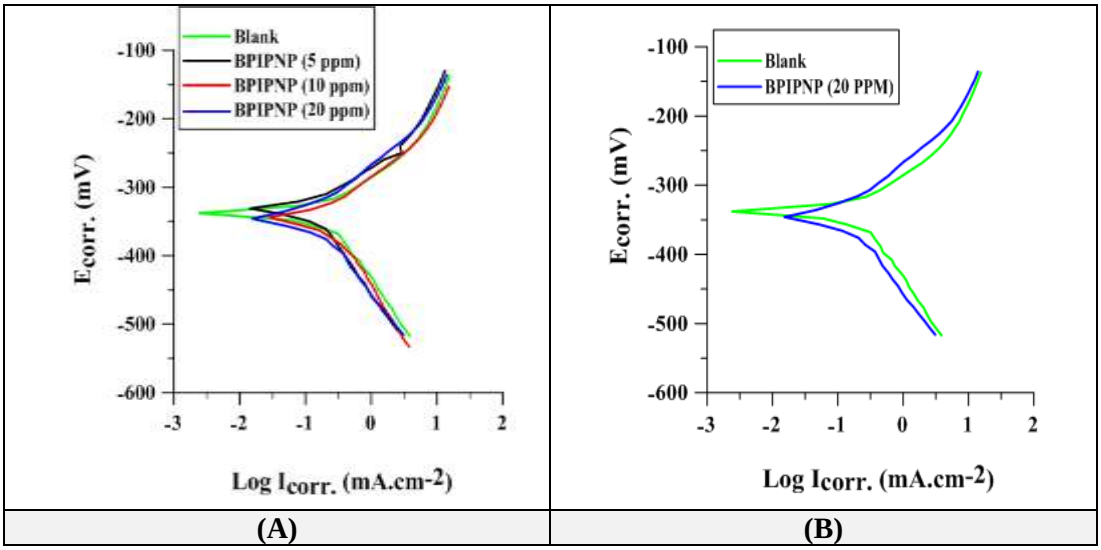

(A) **(B)**

Figure 6-Polarization curve of C.S in 0.5M HCl for (BPIPNP**)** compound; (A) at different concentrations and T (of 293K), (B) at the optimum concentration of (BPIPNP**)** compound at T (of 293K).

Corrosion kinetic and thermodynamic activation parameters

Arrhenius equation (Equation 12) was used to study the effect of temperature on the inhibited corrosion reaction carbon steel.

$$\text{Log } (I_{corr}) = \text{Log } A - Ea / 2.303RT \quad \ldots.(12)$$

Where Ea is the energy activation of the corrosion reaction (kJ mol^{-1}) and A is the pre-exponential factor (in molecules cm^{-2} s^{-1}), R is the gas constant and T is the absolute temperature (Kelvin). Values

of Ea were derived from the slopes of linear relationship between (log icorr) versus (1/T), and (A) obtained from the intercepts, see Figures- 7 and 9 for salty and acidic media respectively.

A plot of log (CR/ T) against (1/ T) (Equation 14) gave linear relationship with a slope of (−ΔH*/ 2.303R) and an intercept of [log(R/ Nh) + (ΔS*/ 2.303R)], see Figures- 8 and 10 for salty and acidic media, from which the activation thermodynamic parameters (ΔH* and ΔS*) were calculated, Table - 6.

$$\text{Log (CR/ T)} = \text{Log (R/ N h)} + \Delta S^*/ 2.303R - \Delta H^*/ 2.303RT \quad (14)$$

Where (CR) is the corrosion current density, (R) is the universal gas constant (8.314 J mol^{-1} K^{-1}), (T) is the absolute temperature in K, (h) is the Planck's constant (6.626 x 10^{-34} J s), (N) is the Avogadro's number (6.022 x 10^{23} mol^{-1}), ΔH* is the enthalpy of activation and ΔS* is the entropy of activation.

The enthalpy changes values (ΔH*) of the corrosion reaction in 3.5% NaCl and acidic media are positive values that give an indication of endothermic nature for this reaction [24]. Negative values of the entropy (ΔS*) for corrosion process meaning a decrease in the degree of freedom and a consequent restriction of the corrosion process. The values of ΔG* for corrosion process were calculated from the following relation:

$$\Delta G^* = \Delta H^* - T\,\Delta S^* \quad \ldots.(15)$$

Table 6- Corrosion kinetic parameters for carbon steel in sea water (3.5% NaCl) for blank and with various concentrations of the inhibitor.

Conc. (ppm)	ΔG kJ/ mol				ΔH* kJ/ mol	ΔS* kJ/ mol K	Ea kJ/ mol	A Molecule/ cm^2 S
	293K	303K	313K	323K				
Blank	63.042	64.952	66.862	68.772	7.079	-0.191	9.635	1.10305E+27
5	68.000	69.750	71.500	73.250	16.725	-0.175	19.281	7.20438E+27
10	68.580	69.036	71.220	72.540	29.904	-0.132	32.955	1.29002E+30
20	68.215	69.335	70.455	71.575	35.399	-0.112	32.460	1.55810E+31

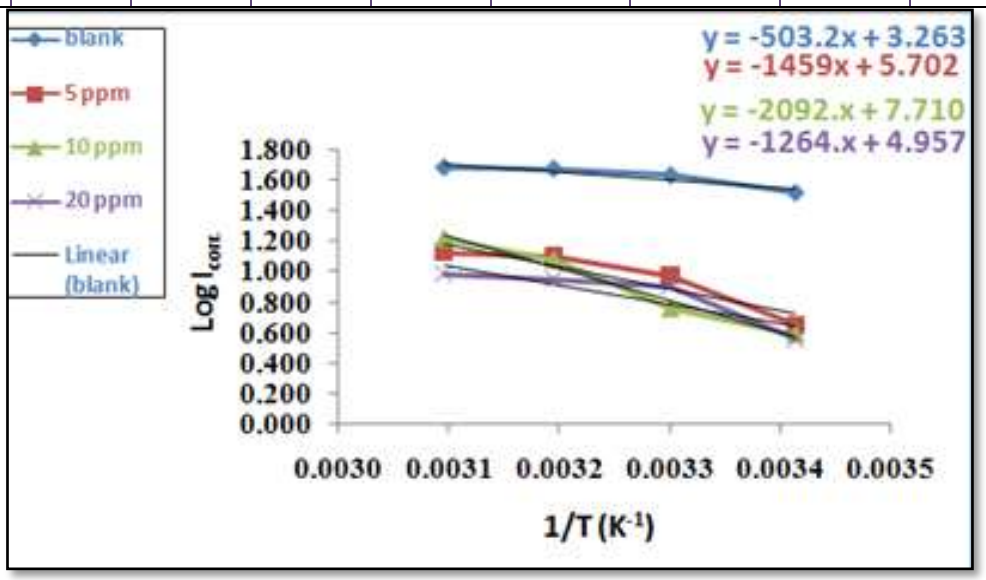

Figure 7- Plot for log (Icorr) vs (1/ T) of carbon steel in sea water for blank and in presence different concentrations of the inhibitor.

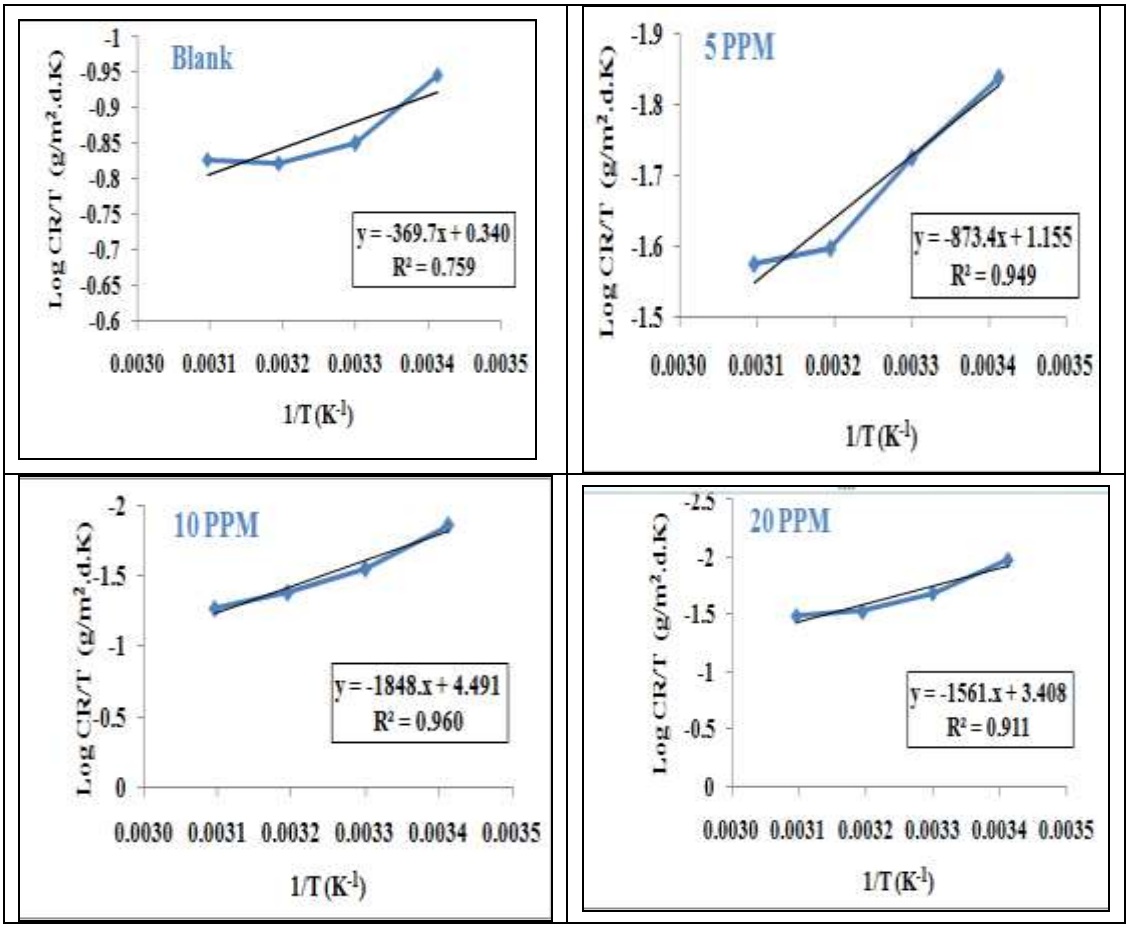

Figure 8-Plot for log (CR/ T) vs (1/ T) of carbon steel in sea water for blank and in presence- different concentration of inhibitor

Table 7- Corrosion kinetic parameters for carbon steel in acidic medium for blank and with various concentrations of the inhibitor.

Conc. (ppm)	ΔG (kJ/ mol)				ΔH* kJ/ mol	ΔS* kJ/ mol K	Ea kJ/ mol	A Molecule/ cm^2 S
	293K	303K	313K	323K				
Blank	62.352	63.742	65.132	66.522	21.625	-0.139	24.181	6.14810E+29
5	66.287	67.297	68.307	69.317	36.694	-0.101	39.250	5.94485E+31
10	66.112	67.132	68.152	69.172	36.226	-0.102	38.783	5.21364E+31
20	66.503	67.513	68.523	69.533	36.910	-0.101	39.466	5.61747E+31

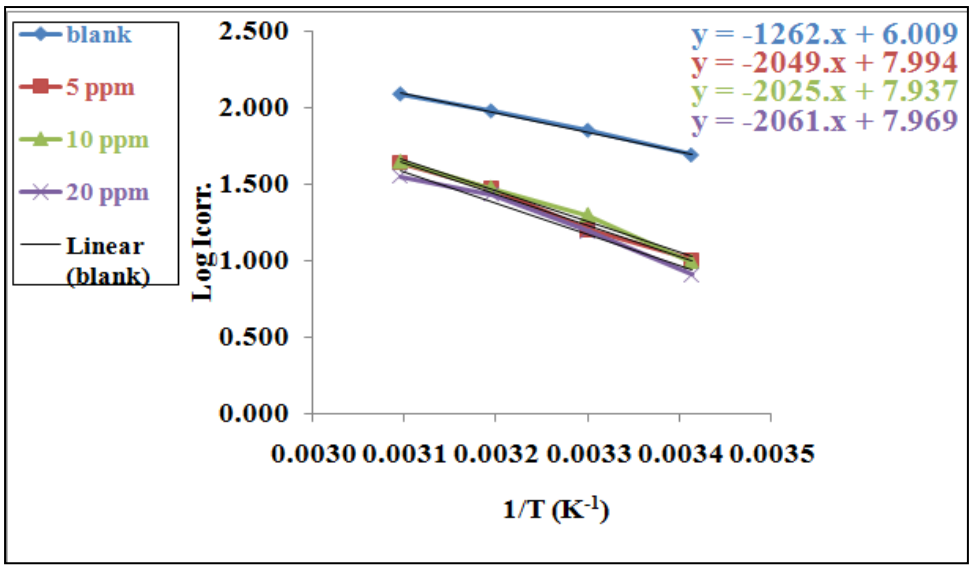

Figure 9-Plot for log (I_{corr}) vs (1/ T) of carbon steel in acidic medium for blank and in presence different concentrations of the inhibitor/

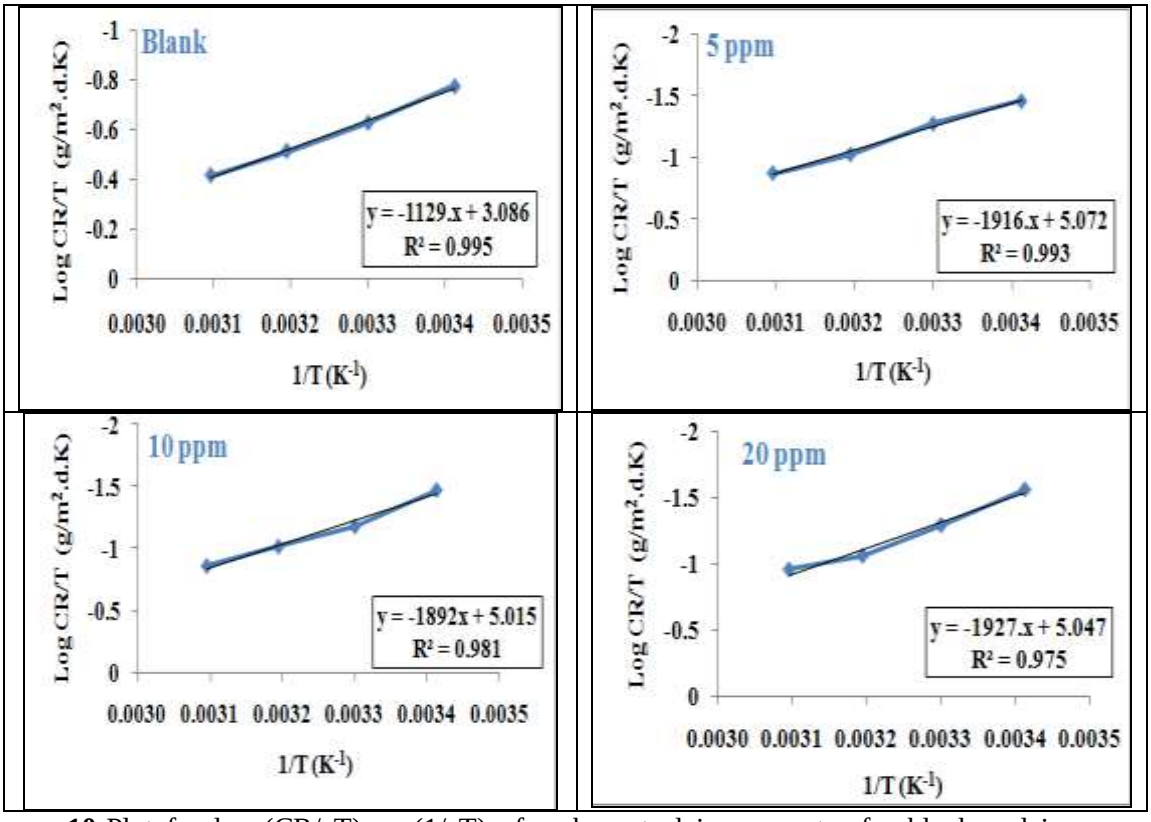

Figure 10-Plot for log (CR/ T) vs (1/ T) of carbon steel in sea water for blank and in presence different concentration of the inhibitor

Adsorption isotherm

The adsorption isotherms are useful to describe the reaction between the inhibitor molecules with carbon steel surface. Langmuir adsorption isotherm can be represented by the following Equation [14].

$$C/\Theta = (1/K_{ads}) + C \quad (14)$$

C: is the concentration of the inhibitor in 3.5% NaCl solution and in 0.5M HCl solution. K_{ads}: is the adsorption/ desorption equilibrium constant.

A plot of C/ θ versus C in the salt and acidic media, could be used to determine the equilibrium adsorption constant K_{ads} for both solutions, Figures- 12 and 14. Figures- 11 and 13, and Tables- 8 and 9 show Langmuir isotherms functions of the adsorption process. The ΔG_{ads} was calculated using Equation (15) [15].

$$\Delta G_{ads} = -2.303\ RT\ Log\ (55.55K_{ads}) \quad (15)$$

Whereas R is the gas constant (J K^{-1} mol^{-1}), T is the absolute temperature (K), and 55.5 is the molar concentration of water (mol L^{-1}) in solution. By plotting K_{ads} versus (1/ T) the $\Delta G°_{ads}$ was extracted from the slope. The entropy and enthalpy adsorption values were obtained by using Equations (15, 16), as shown in Figure-12 for the salt medium and Figure-14 for the acidic medium.

$$\Delta G°ads = -RT \ln Kads \quad (16)$$

$$\Delta G°ads = \Delta H°ads - T\Delta S°ads \quad (17)$$

The negative values of the $\Delta G°_{ads}$ reflect the spontaneous adsorption. In general, values of $\Delta G°_{ads}$ higher than (-40 kJ mol^{-1}) are compatible with physisorption and those lower than (-40 kJ mol^{-1}) involve chemisorptions [16]. The calculated values for $\Delta G°_{ads}$ were found in the range of (-12.250 to -9.817 kJ mol^{-1}) at different temperatures (293-323K) in the salt media, while, $\Delta G°_{ads}$ were found in the range of (-11.279 to -8.966 kJ mol^{-1}) at different temperatures (293-323K) in the acidic medium. These values fall between the threshold values for the physisorption. The entropy $\Delta S°_{ads}$ value was positive confirming that the corrosion process is entropically favorable [25]. The negative value of $\Delta H°_{ads}$ in the salt and acidic media indicates the adsorption of inhibitory compounds on the C.S surface is an exothermic process. For compound **(**BPIPNP**)** $\Delta H°_{ads}$ is equal to (-25.369 kJ mol^{-1}) in the salt medium, while, the acidic medium have $\Delta H°_{ads}$ is equal to (-20.506 kJ mol^{-1}).

Table 8- Thermodynamic parameters for adsorption of **(**BPIPNP**)** compound on C.S surface in 3.5% NaCl solusion at various temperatures.

T (K)	K_{ads} (L mol^{-1})	$\Delta G°_{ads}$ (kJ. mol^{-1})	$\Delta H°_{ads}$ (kJ.mol^{-1})	$\Delta S°_{ads}$ (kJ.mol^{-1})	R^2
293	1.212 x 10^6	-12.250	-25.369	0.065	0.999
303	1.650 x 10^6	-13.013			0.997
313	1.149 x 10^6	-12.116			0.992
323	4.544 x 10^6	-9.817			0.970

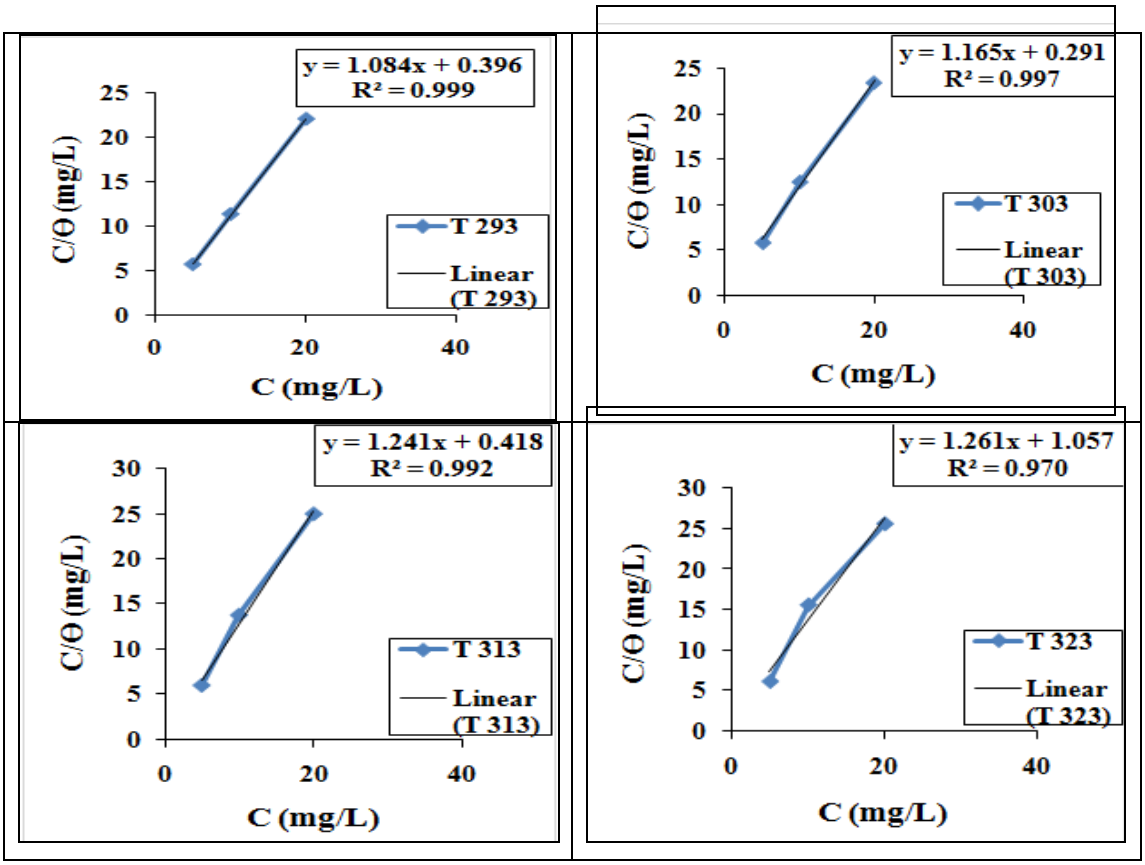

Figure 11-Langmuir isotherms plot for the adsorption BPIPNP compound on carbon steel in the salt medium at the temperature range of (293, 303, 313 and 323) K.

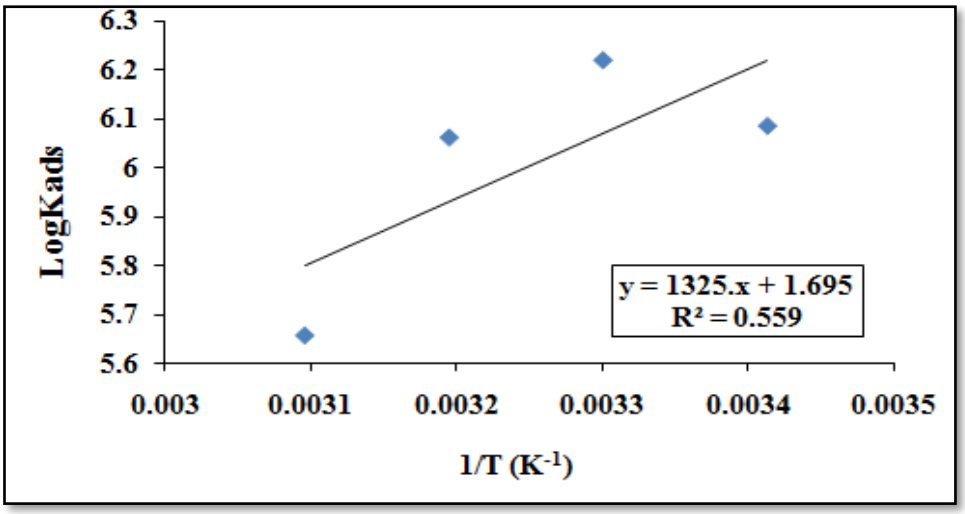

Figure 12-Plot of log Kads vs (1/ T) for (BPIPNP**)** compound in the salty medium

Table 9- Langmuir parameters for adsorption of (BPIPNP**)** compound on carbon steel surface in 0.5M HCl solution at different temperature/

T (K)	K_{ads} (L mol^{-1})	$\Delta G°_{ads}$ (kJ. mol^{-1})	$\Delta H°_{ads}$ (kJ.mol^{-1})	$\Delta S°_{ads}$ (kJ.mol^{-1})	R^2
293	8.196 x 10^5	-11.279	-20.506	0.077	0.999
303	7.709 x 10^5	-11.127			0.996
313	8.780 x 10^5	-11.449			0.999
323	3.022 x 10^5	-08.966			0.996

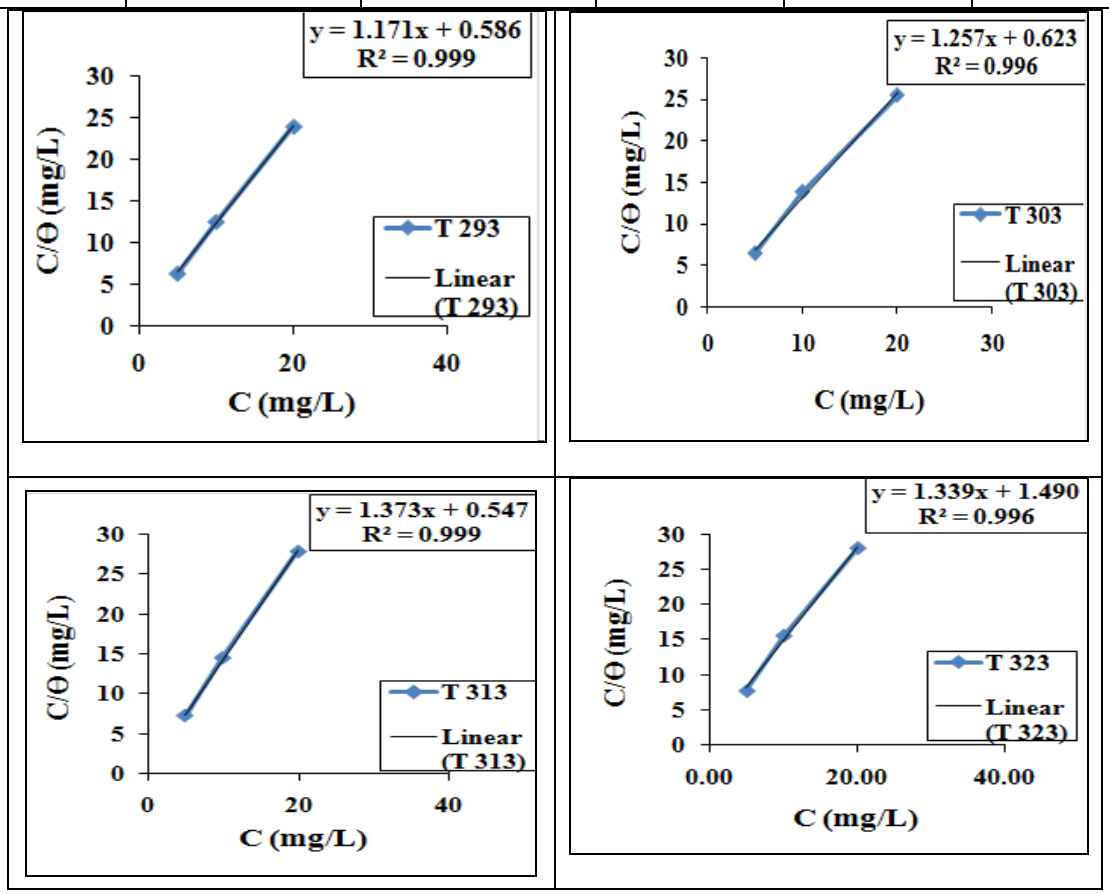

Figure 13-Langmuir isotherms plot of the adsorption of inhibitor (BPIPNP) on carbon steel in the acidic medium at the temperatures of (293, 303, 313 and 323) K.

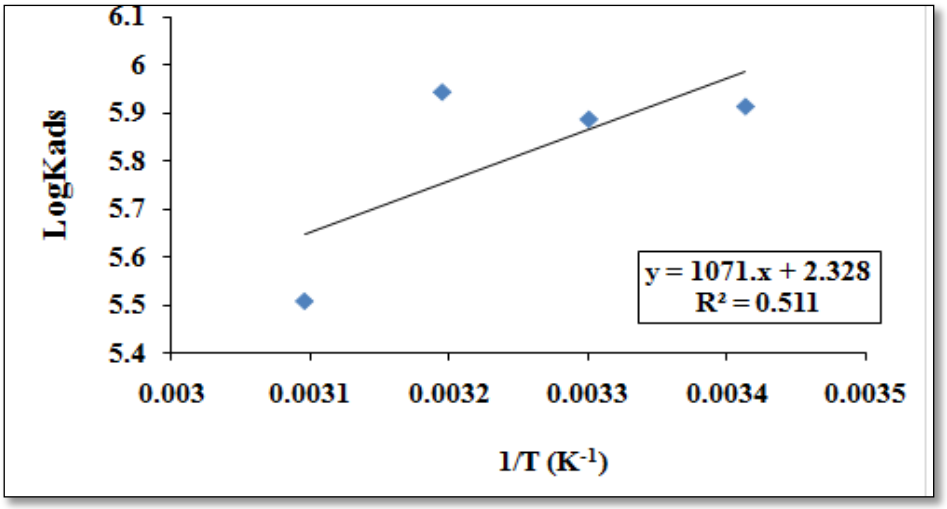

Figure 14-Plot of log Kads vs (1/ T) for (BPIPNP**)** inhibitor in the acidic medium

Scanning Electron Microscopy (SEM)

In Figures-(15a, 16a) the badly damaged surface obtained when the metal was remained immersed in saline water and acidic solution respectively. However, Figures- (15b, 16b) shown C.S surface in the presence of inhibitor (BPIPNP) in saline water and in acidic solution had respected smoothness as compared to Figures-(15a, 16a), indicating reduction of the corrosion rate. This improvement in surface morphology is due to the formation of a protective film of compound (BPIPNP) inhibitor on the C.S surface which is represent for inhibition of corrosion [26].

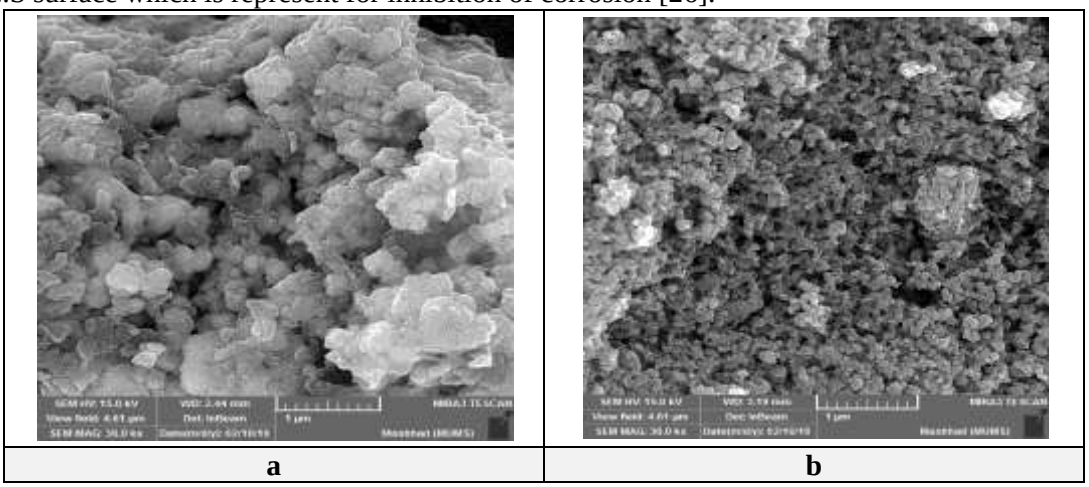

a	b

Figure 15-SEM images of carbon steel in salt medium of 3.5% NaCl solution at 293 K (a) without (BPIPNP) inhibitor (b) in presence of 20 ppm (BPIPNP) inhibitor.

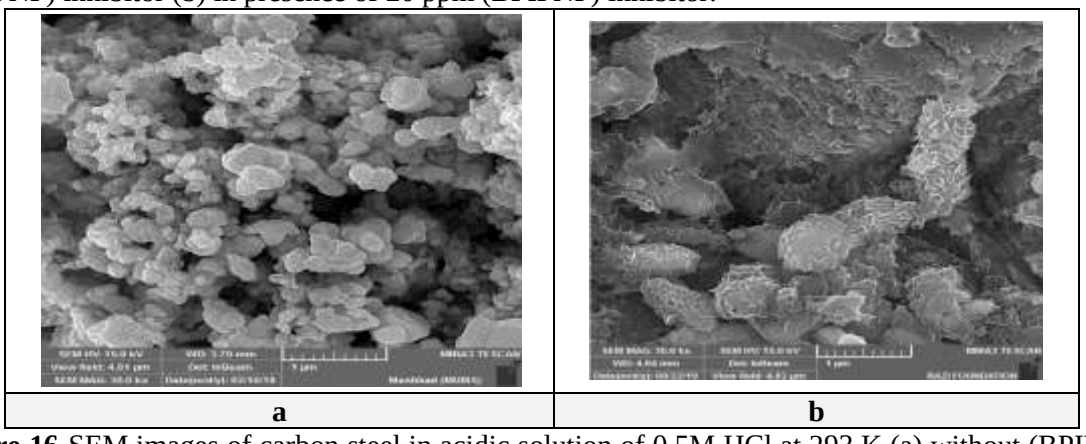

a	b

Figure 16-SEM images of carbon steel in acidic solution of 0.5M HCl at 293 K (a) without (BPIPNP) inhibitor (b) in presence of 20 ppm (BPIPNP) inhibitor.

Atomic Force Microscopy (AFM)

Surface morphology of carbon steel samples in a salt medium of 3.5% NaCl solution and 0.5M HCl solution in the absence and presence of the optimum concentration (20 ppm) of compound (BPIPNP) were investigated by AFM. The results are shown in Figures-(17(a-d), 18(a-d)). The average roughness is clearly shown in Figures- (17(a-b), 18(a-b) that carbon steel sample is badly damaged due to the 3.5% NaCl salt or 0.5M HCl attack on its surface. The average roughness (S_a) for the carbon steel surface is 3.97nm and 178nm in salt and acid solutions respectively without the presence of the inhibitor. The (S_a) was reduced to 1.64nm and 1.71nm in the presence of the optimum concentration (20 ppm) of (BPIPNP) compound, as shown in Figures-(17 c,d), (18 c,d), that display the carbon steel surface after immersion in salt and acidic media [27].

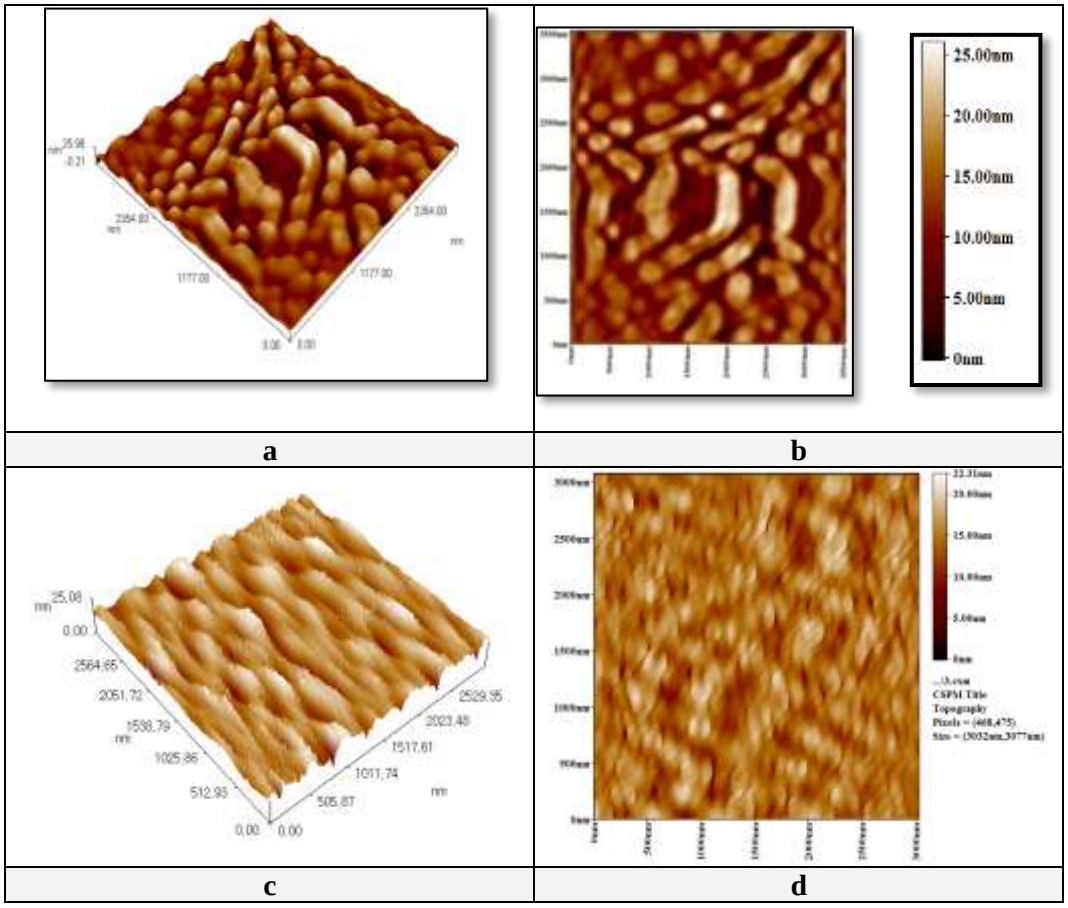

Figure 17-AFM of C.S surface (a, b) in salt medium of 3,5% NaCl solution without presence of the (BPIPNP) inhibitor, (c, d) in presence of 20 ppm of (BPIPNP) inhibitor.

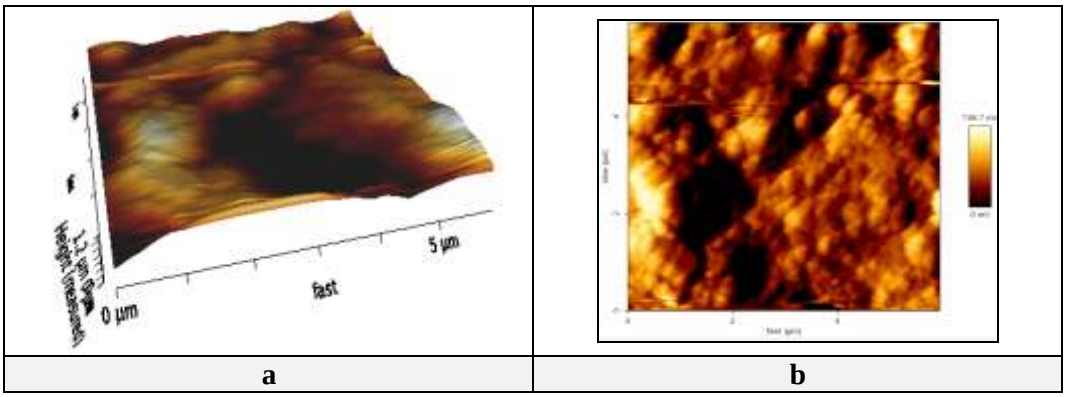

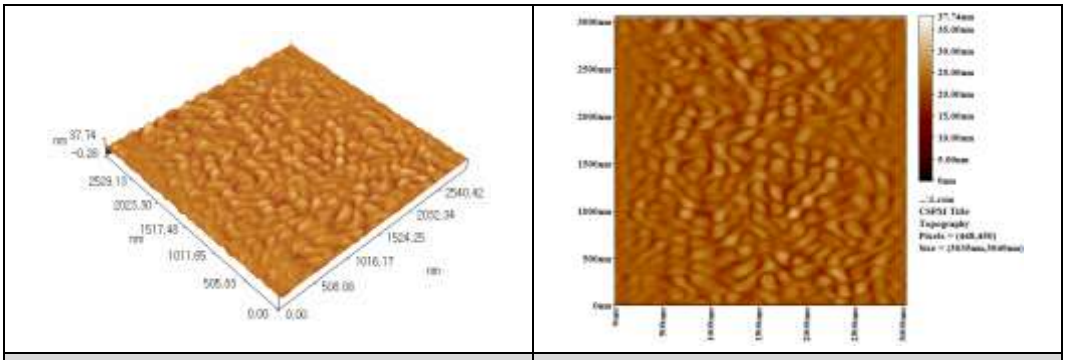

c **d**

Figure 18-AFM of C.S surface (a, b) in acidic solution without presence of the (BPIPNP) inhibitor, (c ,d) in presence of 20 ppm of (BPIPNP) inhibitor.

Conclusions

- The new synthesized imidazolidine 4-one (BPIPNP) derivative was theoretically found to be a good organic corrosion inhibitor for carbon steel in both saline and acidic media.
- The inhibition efficiency were measured for (BPIPNP) derivative experimentally using potentiodynamic polarization measurements reflected that the studied inhibitor (BPIPNP) could be classified as a mixed inhibitor in both saline and acidic media.
- The inhibition efficiency increased with increasing the inhibitor concentration and decrease with increase temperature (physisorption inhibition).
- The inhibition efficiency for corrosion of carbon steel by using (BPIPNP) inhibitor is higher in salty medium than in acidic medium.
- The adsorption of (BPIPNP) compound on C-steel follows the Langmuir adsorption isotherm model.
- The high values of K_{ads} indicate a good corrosion inhibition of carbon steel in salty and acidic media by BPIPNP.
- The ($\Delta G°_{ads}$) values indicate the inhibition process to be a physical adsorption process.

References

1. Corrosão, V.G. **2007**. 5th Eddition. Rio de Janeiro, S.A.: Livros Técnicose Científicos,.
2. David, A. **2017**. Predicting the performance of organic corrosion inhibitors. *Metals*, **7**(553): 1-8.
3. Liang, C., Xia, J., Lei, D., Li, X., Yao Q. and J. Gao. **2014**. Synthesis, in vitro and in vivo antitumor activity of symmetrical bis-Schiff base derivatives of isatin. *Eur. J. Med. Chem*. **74**: 742-50.
4. El Bakri, Y., Boudalia, M., Echihi, S., Harmaoui, A., Sebhaoui, J., Elmsellem, H., Ramli, Y., Guenbour, A., Bellaouchou, A. and Essassi, E. **2017**. Performance and theoretical study on corrosion inhibition of new Triazolopyrimidine derivative for Carbon steel in hydrochloric acid. *Journal of materials and Environmental Sciences*, **8**(2): 378-388.
5. Sallom, K.J. **2019**. Synthesis and biological activity evaluation of new imidazo and bis imidazo (1,2-a) pyridine derivatives. M.Sc Thesis, University of Baghdad, College of Science, Baghdad, Iraq,
6. Al-Lami, N. and Salom, K.J. **2018**. Synthesis and biological activity evaluation of new imidazo and bis imidazo (1,2-A) pyridine derivatives. *J. Glob. Pharm. Tech.*, **10**(11): 603-611.
7. Duboscq, J., Sabot, R., Jeannin M. and Refait, P. **2018**. Localized corrosion of carbon steel in seawater: Processes occurring in cathodic zones. *Materials and Corrosion*, **70**(6): 941-1140.
8. Rajendran, M., Keerthika, K., Kowsalya, M. and Devapiriam, D. **2016**. Theoretical studies on corrosion inhibition efficiency of pyridine carbonyl derivatives using DFT method. *Der Pharma. Chemica.*, **8**(3): 1-79.
9. Ahmed, A.H., Kubba R.M. and Al-Majidi S.M.H. **2018**. Synthesis, identification, theoretical and experimental studies of carbon steel corrosion inhibition in sea water by some new diazine derivatives linked to 5-nitro isatin moiety. *Iraqi Journal of Science*, **59**(3B): 1347-1365.

10. Becke, A. **1993**. Density-functional thermochemistry. III. The role of exact exchange. *Journal of Chem. and Phys.* **98**: 5648-5652.
11. Kubba R.M. and Mohammed, M. **2016**. Theoretical studies of corrosion inhibition efficiency of two new N-phenyl-ethylidene-5-bromo isatin derivatives. *Iraqi Journal of Science*, **57**(2B): 1041-1051.
12. Zhang, J., Liu, J., Yu, W., Yan, Y., You, L. and Liu, L. **2010**. Molecular modeling of the inhibition mechanism of 1- (2-aminoethyl)-2-alkyl-imidazoline, *Corros. Sci.,* **52**(6): 2059-2065.
13. Dewar, M.J.S. and Thiel, W. **1977**. Ground states of molecules. 38. The MNDO method. Approximations and parameters. *J. Am. Chem. Soc.* **99**: 4899-4907.
14. Singh, A., Ansari, K.R., Lin, Y., Quraishi, M.A., Lgaz, H. and Ill-Min Chung. **2019**. Corrosion inhibition performance of imidazolidine derivatives for J55 pipeline steel in acidic oilfield formation water: Electrochemical, surface and theoretical studies. *J. of Taiw. Inst. of Chem. Eng.,* **95**: 341-356.
15. Kubba, R.M., Challoob, D.A and Hussen, S.M. **2017**. Quantum mechanical and electrochemical study of new isatin derivative as corrosion inhibitor for carbon steel in 3.5 % NaCl. *Int. J. of Sci. and Res,* **6**(7): 1656-1669.
16. Louadi, Y.E., Abrigach, F., Bouyanzer, A., Touzani, R., El Assyry, A., Zarrouk, A. and Hammoutia, B. **2017**. Theoretical and Experimental Studies on the Corrosion Inhibition Potentials of Two Tetrakis Pyrazole Derivatives for Mild Steel in 1.0M HCl. *Portugaliae Electrochimica Acta*, **35**(3): 159-178.
17. Kubba, R.M. and Alag**,** A.Sh. **2017**. Experimental and Theoretical Evaluation of new Quinazolinone Derivative as Organic Corrosion Inhibitor for Carbon Steel in 1M HCl Solution. *IJSR*, **6**(6): 1832-1843.
18. Speicher, C. and Dreizler, R. **1998**. Density functional Approach to quantum hadrodynamics: theoretical foundations and construction of extended thomas- fermi models, *Ann. of Phys*., **213**: 312-354.
19. Khaled, K.F. **2010**. Studies of iron corrosion inhibition using chemical, electrochemical and computer simulation techniques. *Electrochimica Acta*. **55**: 6523–6532.
20. Raafat, M., Mohamed, K. and Faten, M. **2008**. Quantum chemical studies on the inhibition of corrosion of copper surface by substituted uracils. *Applied Surface Science*, **255**: 2433-2441.
21. Poorqasemi, E., Abootalebi, O., Peikari, M., Haqdar, F. **2009**. Investigating accuracy of the Tafel extrapolation method in HCl solutions, *Corros. Sci*. **51**: 1043– 1054
22. Kaskah, S.E. **2018**. Surface protection of steel CR4 by using N-acyl sarcosine derivatives in salt water. Ph.D Thesis, Universität Koblenz-Landau.
23. Hong, S., Chen, W., Luo, H.Q. and Li, N.B. **2012**. Inhibition effect of 4-amino-antipyrine on the corrosion of copper in 3 wt. % NaCl solution, *Corro. Sci.*, **57**: 270–278.
24. Ben Hmamou, D., Aouad, M., Salghi, R., Zarrouk, A., Assouag, M., Benali, O., Messali, M., Zarrok, H. and Hammouti, B. **2012**. Inhibition of C38 steel corrosion in hydrochloric acid solution by 4,5- diphenyl-1H-imidazole-2-thiol:gravimetric and temperature effects treatments. *Int. J. of Sci. and Res.* **4**(7): 3498-3504.
25. Abd-El-Naby, B., Abdullatef, O., Khamis, E. and El-Mahmody, W. **2016**. Effect of cetyl trimethyl ammonium bromide surfactant as novel inhibitor for the corrosion of steel in 0.5 M H_2SO_4. *Int.J. Electrochem.and Sci.* **11**: 1271-1281.
26. Mohamed, A., Khaled, Z., Hamdy, A., Abo-Elenien, O. and Olfat, E. **2015**. Synthesis of novel schiff base silicon compound for employing as corrosion inhibitor for carbon steel in the 1 M HCL and 3.5% NaCl aqueous media. *International Journal of Chemical, Environmental & Biological Sciences*, **3**: 2320-4087.
27. Gowri, S., Sathiyabama, J., Prabhakar, P. and Rajendran, S. **2012**. Inhibition behaviour of carbon steel in sea water in the presence of tyrosine- Zn^{2+} system. *International Journal of Research in Chemistry and Environment*, **3**: 156-162.